Journal of Physics: Conference Series **3224** (2026) 032090 doi:10.1088/1742-6596/3224/3/032090

The Influence of the Tower and Nacelle in Actuator Line Simulations of Floating Offshore Wind Turbines

Dylan Green[1], Markella Zormpa[1] and Christopher Vogel[1]

[1]Department of Engineering Science, University of Oxford, Oxford, UK

E-mail: dylan.green@eng.ox.ac.uk

Abstract. The platform motions of floating offshore wind turbines generate unsteady wake dynamics that affect downstream power production and fatigue loading. Modelling floating wind farm performance therefore requires an improved understanding of these wake dynamics. However, the aerodynamic influence of the tower and nacelle is commonly neglected in numerical simulations. This study has two objectives: (i) identify the influence of the tower and nacelle on wake dynamics for different platform motions, and (ii) quantify the ability of lower-fidelity meshless methods as a means to avoid costly dynamic meshing. The results demonstrate that while blade-scale effects associated with the tower and nacelle are not fully resolved by lower-fidelity methods, the dominant platform-induced wake dynamics are captured well. Furthermore, the impact of the tower and nacelle model on wake coherence appears to depend on the platform motion degree of freedom: for the motion frequencies and amplitudes explored, inclusion of the model amplifies wake meandering for rolling, while pitching-induced wake dynamics are largely unaffected.

1. Introduction

In recent years, the floating offshore wind energy sector has seen rapid growth, with farm-scale deployment now commencing [1]. As a result, minimising sources of inefficiency, such as wake losses, has become increasingly important. Achieving this requires an understanding of the complex wake dynamics induced by unsteady floating platform motions. Due to the large range of spatial and temporal scales present, Blade-Resolved (BR) simulations become prohibitively expensive. As a result, reduced-order models such as the, Actuator Line Method (ALM) [2], are commonly used for virtual blade representation [3–5]. However, this blade-only modelling strategy typically neglects potentially important aerodynamic effects associated with the tower and nacelle.

The influence of the tower and nacelle aerodynamics has been investigated for fixed-bottom wind turbines. [6] demonstrated that the interaction between the tower wake and the rotation of the rotor wake induces downstream wake asymmetry. [7] observed enhanced wake meandering when a nacelle model was employed. At utility scale, the tower was shown to disrupt the formation of coherent vortex sheets in the turbine wake [8]. [9] showed that the tower and nacelle cause deviations from the Gaussian profile assumed by many wake models. [10] showed that low-frequency modes, generated through nonlinear interactions between the tip and tower shed vortices, contribute to wake recovery.

The introduction of floating platform motions adds further complexity to the role of the tower and nacelle in shaping wake dynamics through the addition of platform motion related

timescales. Accordingly, the present study has two primary objectives: (i) to compare meshless and body-conforming approaches for modelling the tower and nacelle as a means to alleviate the requirements of dynamic mesh methods, and (ii) to identify how prescribed platform motion characteristics influence the impact of the tower and nacelle on wake dynamics.

The remainder of the paper is organised as follows. Section 2 describes the numerical setup, including the tower and nacelle modelling approaches and the mesh convergence test. Section 3 presents comparisons with recent experimental measurements and BR numerical simulations, before applying the methodology to examine the influence of the tower and nacelle under two representative prescribed platform motion cases. Finally, Section 4 summarises the main findings and outlines directions for future work.

2. Methodology

2.1. Test case

The NETTUNO experimental campaign was selected as the validation case owing to the availability of recent experimental measurements and BR simulation results. The campaign was conducted using a 1:75 scale model turbine subject to prescribed sinusoidal motions in low-turbulence (intensity $\approx 2\%$), uniform inflow conditions [11]. The imposed platform motions are characterised by a reduced frequency $f_p^\star = f_p D/U_\infty$ and amplitude A_p, where f_p denotes the platform-motion frequency, D the rotor diameter (2.38 m), and U_∞ the freestream velocity ($4\,\mathrm{m\,s^{-1}}$). The wind tunnel section had a width and height of $5.28D$ and $1.61D$ respectively, resulting in a blockage of 8.4%. To study solely the aerodynamic response of the turbine to prescribed motions, the turbine was operated at fixed blade pitch and constant rotational speed.

2.2. Numerical setup

The numerical setup is configured to replicate the NETTUNO experimental test conditions. The wind tunnel blockage is approximated using a wall-modelled approach to replicate the effects of the wall boundary layers. The inflow turbulence is reproduced using the divergence-free synthetic eddy method of [12]. Turbulence is modelled using Large Eddy Simulation (LES) employing the wall-adapting local eddy-viscosity for turbulence closure [13]. Here, LES was selected for its superior accuracy in resolving platform-motion-induced wake dynamics compared with alternatives such as unsteady Reynolds-averaged Navier–Stokes simulations [5]. The transport equations are solved with a limited second-order finite volume method using the pressure implicit split operator method.

The turbine blades are modelled using the ALM, which treats them as momentum source terms based on tabulated lift and drag coefficients. This approach removes the need to resolve the fine-scale geometry necessary for accurately capturing blade flows and has been previously used to model floating turbine wake dynamics [4]. [3] demonstrated that the ALM has a tendency to overpredict the tip vortex core radius while underpredicting its strength when compared to alternatives such as free vortex wake methods. Although this remains a limitation of the approach, the underlying finite volume framework enables the use of synthetic eddy methods for turbulence reproduction and thus a better representation of interaction between the freestream and the wake, potentially outweighing these limitations. The ALM used in this study was previously validated for bottom-fixed and floating turbines [14–16]. The potential flow velocity sampling method of [17] is used to compute the forces of the virtual blades, which are then convolved with a Gaussian kernel of width $\varepsilon = 2\Delta$, where Δ is the cell size. Sampling was performed outside the primary force-imposition region, at a radius of $r_s = 3.3\varepsilon$. The timestep was selected to be the maximal value such that the blade tip does not travel more than a cell size in a time step, $\Delta t < \Delta/\pi D f_r$, and satisfies $f_r \Delta t = i \in \mathbb{N}$, where f_r is the rotor frequency.

In the present study, two methods for representing the dynamic motions of the tower and nacelle are investigated: a Dynamic Mesh Method (DMM), and an Immersed Boundary Method (IBM). The former solves a mesh displacement equation $\nabla \cdot (\gamma \nabla \boldsymbol{d}) = 0$, where $\boldsymbol{d}$ is the vector describing the point displacement and γ is a diffusivity defined to be the inverse of the distance to the moving body. The solution of the mesh displacement equation is then used to modify the mesh and compute the resultant fluxes. The near-wall behaviour is modelled using a wall model. The IBM is a Brinkman penalisation method as described in [18]. This method applies a forcing described by $\boldsymbol{f} = \chi_s \lambda(\boldsymbol{u} - \boldsymbol{u}_s)$, where $\chi_s \in [0, 1]$ is a mask describing the immersed solid, λ is a penalisation factor, $\boldsymbol{u}$ is the fluid velocity, and $\boldsymbol{u}_s$ is the velocity of the immersed solid. The parameter λ is chosen to supply sufficient forcing without incurring excessive numerical stiffness.

2.3. Mesh convergence

Figure 1 illustrates the mesh refinement employed in the present study. The finest region was designed to adequately resolve near-wake dynamics while limiting the overall cell count. An upstream refinement region extends to the inlet to preserve the transport of small-scale turbulence.

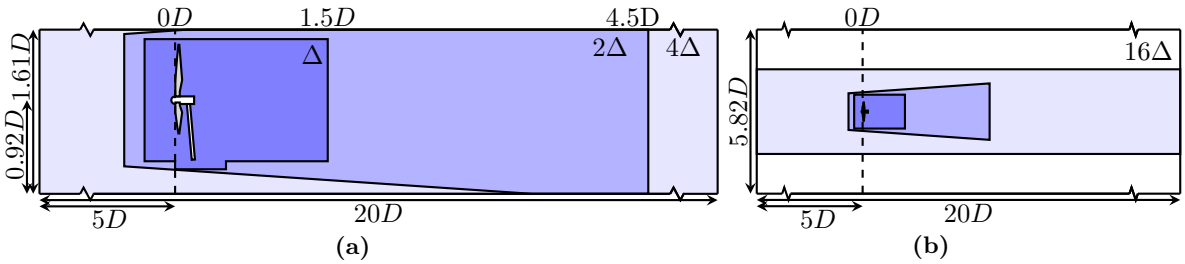

Figure 1. Mesh refinement regions shown from the side (a) and top (b). Inflation layers along the wind tunnel walls are not depicted.

To determine the optimal cell refinement, results from three different mesh resolutions are compared. Each simulation models the same pitching turbine with a DMM tower and nacelle undergoing pitching motions characterised by $f_p^\star = 0.60$ and $A_p = 1.9°$, and subject to uniform laminar inflow. The mesh discretisation in the vicinity of the turbine is given by $D/\Delta = 240, 200$ or 160. Figure 2 depicts the coherent component of the rotor thrust and the streamwise component of the wake at $0.2D$ downstream of the initial rotor plane. The coherent component of the thrust is defined to be $\tilde{T} = \langle T \rangle - \overline{T}$ where $\langle \cdot \rangle$ and $\bar{\cdot}$ denote phase and time averages, respectively, with phase averaging performed over many cycles defining a platform phase $\tau = tf_p \pmod 1 = tf_p - \lfloor tf_p \rfloor$, where t denotes time.

Figure 2a demonstrates that all mesh resolutions produce comparable oscillation amplitudes in the rotor thrust associated with platform motions. However, the amplitude of the tower-shadow effect is overestimated by the coarsest mesh, likely as a result of the larger ALM sampling radius. Good agreement is observed between the two most resolved cases. A small ($< 1\%$) change in the time-averaged thrust is observed between the coarsest and finest meshes; however, this difference is considered negligible and is primarily attributed to the ALM rather than the tower and nacelle modelling.

Figure 2b illustrates the time-averaged mean and standard deviation of the streamwise velocity in the near wake. The mean profiles are generally consistent, although some discrepancies are observed near the wake centreline ($y \approx 0$). The standard deviation is underpredicted by the coarsest mesh while the two finer meshes are in agreement. Based on these results, $D/\Delta = 200$ was selected for all subsequent simulations to avoid unnecessary computational expense. A separate mesh convergence study is not presented for the IBM, as the objective is to compare the

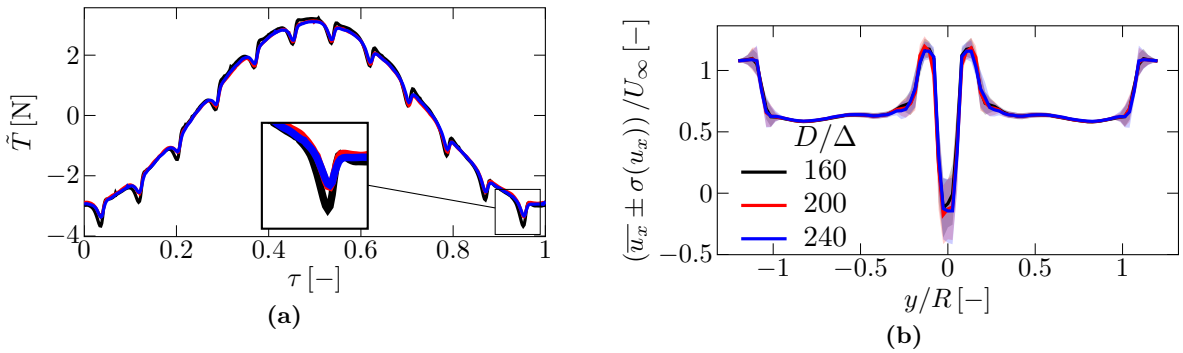

Figure 2. Mesh convergence comparison using three grid resolutions for a pitching turbine with $(f_p^\star, A_p) = (0.60, 1.9°)$. (a) Coherent component of the rotor thrust. (b) Time-averaged mean streamwise velocity profile at $0.2D$ downstream of the rotor plane at hub height, where y is the cross-stream direction and R is the rotor radius. Shaded regions indicate ± 1 standard deviation from the mean.

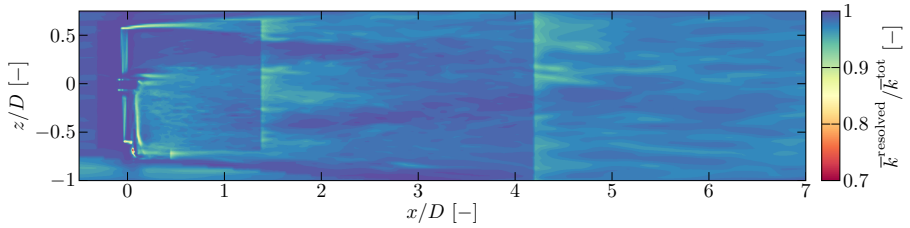

Figure 3. Contour of the ratio of resolved to total turbulent kinetic energy for a pitching turbine with $(f_p^\star, A_p) = (0.60, 1.9°)$ and an IBM tower and nacelle model.

two models on the same background mesh rather than assess their convergence characteristics.

To assess the suitability of the mesh for LES, the ratio of the resolved to total turbulent kinetic energy was evaluated on a streamwise slice, figure 3, for a turbulent inflow simulation. Almost all of the domain resolves greater than 90% of the turbulent kinetic energy with only a small region where the tip vortices meet the tower resolving approximately 70%. This region is confined a few cells and is therefore assumed not to significantly affect the downstream wake development. The use of this mesh resulted in a maximum Courant number of 0.31.

3. Results

3.1. Comparison to experimental & blade-resolved results

The methods are evaluated through comparison with the recent experimental measurements of [11] and the BR numerical simulations of [19]. The experimental data provides validation against the physical response of the system, whereas the numerical simulations provide access to high-fidelity quantities such as the blade spanwise loading distributions. A single case is compared, characterised by pitching motions with $f_p^\star = 1.19$ and $A_p = 0.3°$.

The BR simulations employed a fully body-conforming approach, with the blades, tower, and nacelle explicitly meshed. Rotor rotation and platform motions were modelled using an innovative combined sliding and deforming mesh method. The blade boundary layers were resolved without the use of a wall model, and the RANS equations were closed using the $k-\omega$ SST model [19]. This modelling choice represents a key distinction between the BR reference data and the present work. The ALM framework enables computationally feasible simulations with scale-resolving turbulence closures, at the expense of accuracy in blade load distribution, unsteady aerodynamic response, and near-wake turbulence production.

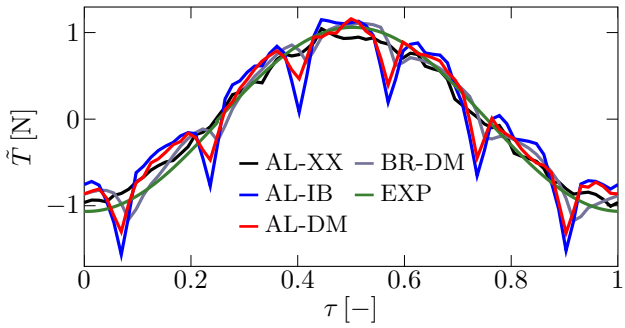

Figure 4. Coherent component of the rotor thrust under pitching motions characterised by $(f_p^\star, A_p) = (1.19, 0.3°)$.

Table 1. Time-averaged thrust and amplitudes of thrust oscillations for a pitching turbine with motions characterised by $(f_p^\star, A_p) = (1.19, 0.3°)$.

	$\overline{T}$ [N]	$\Delta T^{f_p^\star}$ [N]	$\Delta T^{f_b^\star}$ [N]
AL-XX	35.71	0.955	0.027
AL-DM	35.76	0.965	0.207
AL-IB	35.66	0.949	0.325
BR-DM [19]	35.01	1.015	–
EXP [11]	36.19	0.957	–

Figure 4 presents the coherent component of the rotor thrust. Here AL-XX refers to the ALM with no tower and nacelle model, AL-IB and AL-DM correspond to the ALM combined with IBM and DMM representations of the tower and nacelle respectively, BR-DM is the BR data of [19], and EXP refers to the experimental measurements of [11].

Owing to a blade mass imbalance, the experimental measurements are low-pass filtered at a cut-off frequency of $f = 3\,\text{Hz} = 0.75 f_r$. Consequently, no blade-tower interaction can be observed in $\tilde{T}$, and therefore comparisons with EXP are restricted to the rotor response at the platform motion frequency. Furthermore, due to the location of the load cell, the EXP thrust includes contributions from the nacelle.

Focusing first on the response of the rotor to the platform motions, all numerical approaches show good agreement with the experimental data, exhibiting a harmonic response in the rotor thrust with approximately the same amplitude and no appreciable phase differences. This is confirmed by the amplitude of the rotor thrust at the platform reduced frequency, $\Delta T^{f_p^\star}$, tabulated in table 1. The same table indicates agreement in the time-averaged thrust, $\overline{T}$, with all numerical predictions lying within the experimental uncertainty [11].

Differences between the modelling approaches become apparent when examining the amplitude of the thrust oscillation at the blade-passing frequency, $\Delta T^{f_b^\star}$. Both the AL-DM and AL-IB methodologies substantially overpredict the amplitude of the tower-shadow effect relative to the BR reference case. This behaviour can be attributed to the non-local flow sampling performed during the ALM force calculation. The tower-induced velocity deficit pollutes the calculation of the angle of attack and relative velocity used to find the virtual blades' lift and drag forces. Comparing the AL-DM and AL-IB cases further reveals that the AL-IB predicts a significantly stronger thrust oscillation at $f_b^\star$. This can be attributed to the absence of a wall model in the IBM, which results in an excessively thick boundary layer which works to enhance the influence of the tower. The inclusion of a wall model may improve results but at the cost of the ease of implementation and locality of the IBM. A weak oscillatory component at $f_b^\star$ is also observed in the AL-XX case, which is attributed to blade-tip proximity to the wind tunnel ceiling, leading to a small inflow asymmetry.

Figure 5 shows the coherent component of the normal force per unit blade length, $\tilde{F}_n$, at three selected radial blade locations. Consistent with the thrust response discussed previously, both the AL-DM and AL-IB configurations substantially overpredict the tower-blade interaction, which is evident at all radial positions. The response to the platform motion is generally well captured across the span, with the closest agreement observed at the mid-span. The near-hub and near-tip sections show good overall agreement but exhibit noticeable discrepancies, which may be attributed to 3D flow effects present in these regions. These include spanwise flow and

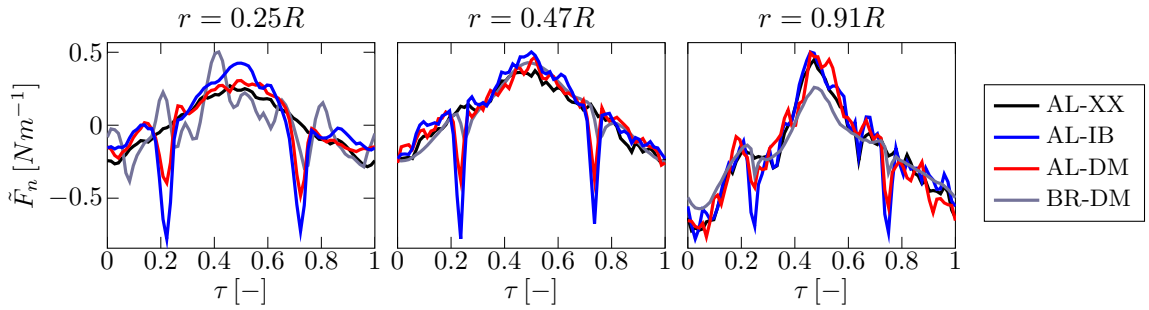

Figure 5. Coherent component of the normal force per unit blade length at three different blade sections ($r = 0.25R, 0.47R, 0.91R$) for the blade in the vertical position at $\tau = 0$ for a pitching turbine with motions characterised by $(f_p^\star, A_p) = (1.19, 0.3°)$.

tip and root vortical structures that cannot be directly resolved by the ALM due to its use of 2D aerofoil polars. The inboard section ($r = 0.25R$) shows noticeable differences between the ALM configurations and the BR data. This is likely due to the ALM's inability to realise dynamic effects such as platform-motion-induced stall that occurs within this region [19].

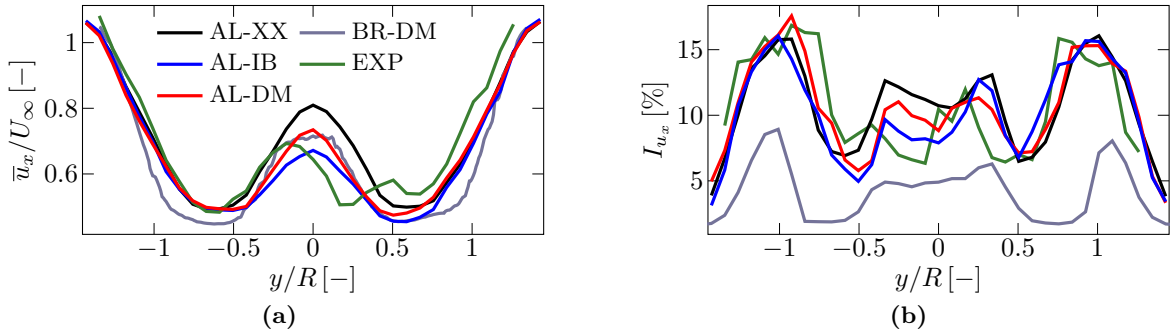

Figure 6. (a) Time-averaged streamwise velocity and (b) turbulence intensity profiles at $3D$ downstream of the initial rotor position for a pitching turbine with motions characterised by $(f_p^\star, A_p) = (1.19, 0.3°)$.

Figure 6 presents the time-averaged streamwise velocity, $\overline{u}_x$, and turbulence intensity, I_{u_x}, at $3D$ downstream from the rotor's initial position. In the absence of a tower and nacelle model, the AL-XX configuration produces an unphysical high-velocity core at the centre of the wake corresponding to a jet. This forms a strong shear layer leading to enhanced turbulence production, as observed in figure 6b. In contrast, the BR-DM, AL-IB, and AL-DM exhibit generally good agreement in the time-averaged velocity profiles, although AL-IB produces a slightly increased velocity deficit. The inclusion of either nacelle representation improves agreement when compared to the experimental results. More pronounced differences are observed in the turbulence intensity profiles. The BR-DM reference data predicts lower wake turbulence levels than the other numerical approaches and the experimental data, which may be attributed to the differences in turbulence modelling strategies. These results suggest that the use of LES in the present study enables a more complete representation of turbulence production and transport in the wake, contributing to improved agreement with the experimental observations.

Overall, results demonstrate that $\overline{T}$ and $\Delta T^{f_p^\star}$ are predicted with excellent agreement relative to the BR and experimental reference data, with both quantities showing little sensitivity to the inclusion of the tower and nacelle models. Phase-averaged blade loads nevertheless reveal a tower-shadow effect that is significantly over-predicted by the ALM configurations relative to

the BR reference data, and discrepancies are observed in the blade load distributions. Despite these differences, the wake-focused results show good agreement with the experimental reference data. The inclusion of a tower and nacelle model improves agreement in both the time-averaged streamwise velocity and turbulence intensity profiles. In particular, the use of LES in the present study enables accurate prediction of downstream unsteady dynamics. These characteristics align well with the scope of the present work, which is concerned with wake evolution rather than blade-scale loading. On this basis, the remainder of the analysis focuses on the AL-IB and AL-DM approaches for the investigation of platform-induced wake dynamics.

3.2. Wake dynamics

Building on the preceding analysis, this section addresses the primary objective of the present study: to assess the impact of tower and nacelle modelling on floating turbine wake dynamics. Two representative motion cases are considered: a pitching turbine and a rolling turbine characterised by $(f_p^\star, A_p) = (0.60, 1.9°)$ and $(0.30, 1.9°)$, respectively. These cases were selected as they are representative of operational platform motions and elicit a strong wake response [20].

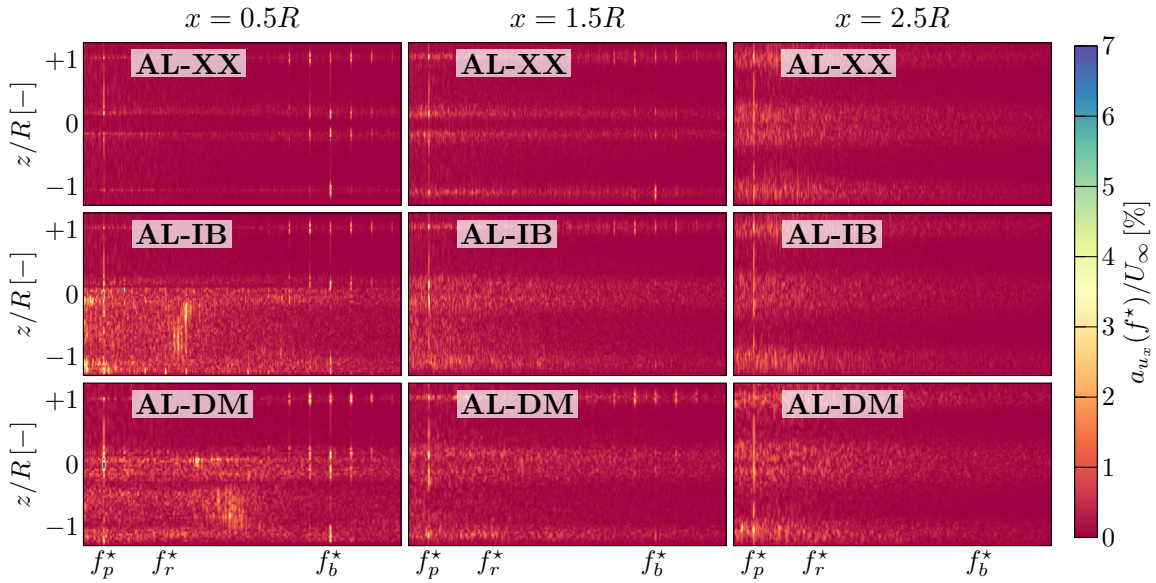

Figure 7. Wake streamwise velocity spectra as a function of the vertical distance, z, relative to the hub height at the initial rotor position for a pitching turbine with $(f_p^\star, A_p) = (0.60, 1.9°)$ at different downstream locations, $x = 0.5R, 1.5R, 2.5R$.

Figure 7 presents the wake streamwise velocity spectra computed over a vertical line at three downstream positions for the pitching turbine case. In the near wake at $x = 0.5R$, the AL-XX spectra exhibit distinct peaks at the platform-motion frequency $f_p^\star$, the blade-passing frequency $f_b^\star$, and their associated combination tones $f_b^\star \pm f_p^\star$ and $f_b^\star \pm 2f_p^\star$. Asymmetry is observed between the upper and lower portions of the wake: the combination frequencies are largely absent in the lower region, while they are pronounced in the upper region. This behaviour arises from the asymmetric platform-induced velocity associated with pitching motion. At $x = 1.5R$ the peaks diminish and are no longer distinguishable by $x = 2.5R$. At this location, a broader spectrum is observed reflecting the onset of the turbulent breakdown of the near wake features. Across the wake a persistent signature at $f_p^\star$ forms as the wake dynamics become increasingly dominated by the platform-motion-induced dynamics. This is in contrast to $x = 0.5R$, where the blade passing frequency and associated coherent tip vortices are a more prominent feature.

Comparing the AL-XX results with those obtained using the AL-DM and AL-IB approaches reveals the distinct differences in the near wake at $x = 0.5R$. In the latter cases, turbulence generated by the tower introduces asymmetry in the wake spectra. Additional spectral content is observed in the frequency range $[f_r^\star, f_b^\star]$, which is likely associated with tower vortex shedding; however, understanding the precise mechanism behind this is challenging given that the tower is immersed within the rotor wake and interacts with the blade-passing flow perturbation. The AL-IB predicts a lower characteristic frequency for this phenomenon, although the amplitude and spectral bandwidth are captured with reasonable agreement.

Remaining at $0.5R$, a pronounced peak at $f_p^\star$ is observed in the vicinity of the nacelle for both the AL-DM and AL-IB cases, suggesting a periodic modulation of the nacelle wake strength induced by the platform motion. The two approaches show reasonable agreement, with the AL-IB slightly underpredicting the oscillation amplitude. In contrast, the AL-XX exhibits a markedly weaker response in this region, demonstrating that it is unable to capture all the dynamics at play. Moreover, the presence of an artificial nacelle jet in the AL-XX case appears to suppress velocity fluctuations near the nacelle, as evidenced by the low-energy band at nacelle height that is absent in the AL-DM and AL-IB results.

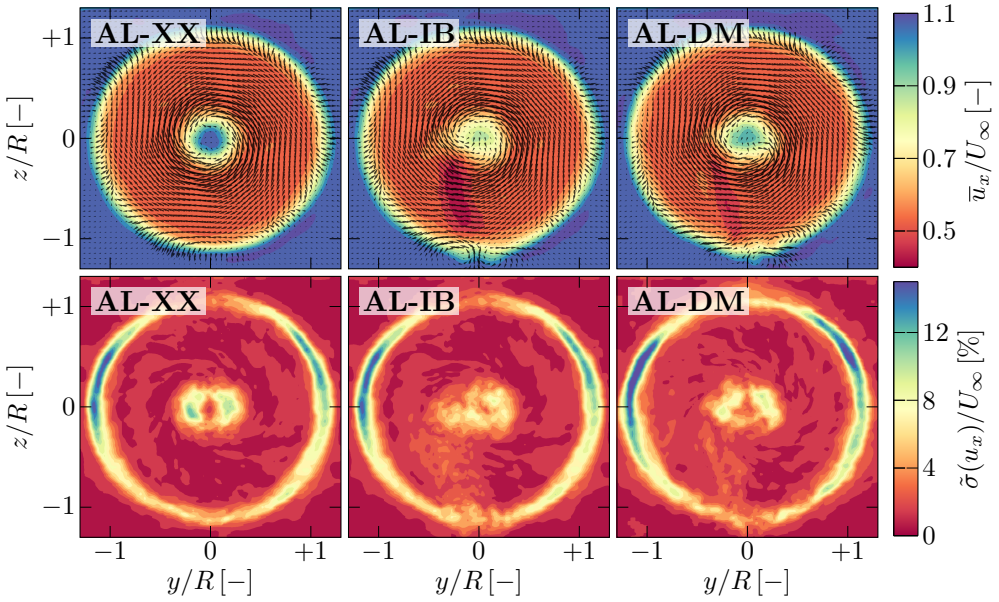

Figure 8. Time-averaged streamwise velocity contour with arrows indicating in-plane time-averaged velocity and coherent standard deviation of the streamwise velocity at $1D$ downstream of the initial rotor position for a rolling turbine with $(f_p^\star, A_p) = (0.30, 1.9°)$.

By $x = 2.5R$, the wake spectra obtained using all modelling approaches show relatively good agreement. At this downstream location, coherent structures generated by the tower and nacelle have either been advected out of the vertical sampling line by the wake rotation or have decayed, resulting in similar spectral characteristics across all cases.

The top row of figure 8 presents contours of the time-averaged streamwise velocity, $\overline{u}_x$, with vectors indicating the in-plane mean velocity for the rolling turbine case. The inclusion of a tower model introduces a local velocity deficit that is subsequently advected by wake rotation, leading to pronounced downstream asymmetry. The magnitude of this deficit is overpredicted by the AL-IB relative to the AL-DM. In addition to the streamwise velocity deficit, the presence of the tower generates non-negligible in-plane velocity components associated with flow diversion

around the structure, as evidenced by the reversal of the in-plane velocity direction compared to the AL-XX configuration. As discussed previously, the inclusion of a nacelle model suppresses the formation of a jet; however, the AL-IB, once again, overpredicts the magnitude of this effect.

The second row of figure 8 shows the coherent standard deviation of the streamwise velocity for the same case. The coherent standard deviation, $\tilde{\sigma}$, is defined as the standard deviation of the phase-averaged quantity and represents the amplitude of the coherent oscillatory component. Near the hub region, the nacelle model reduces the amplitude of the coherent oscillations, which are most pronounced on either side of the wake centreline in the AL-XX configuration. Conversely, the inclusion of the tower model leads to increased coherent fluctuations in the lower left sections of the wake, as indicated by elevated values of $\tilde{\sigma}(u_x)$. These results suggest that the support structure plays a complex role in modulating coherent wake dynamics, simultaneously suppressing and amplifying organised motions.

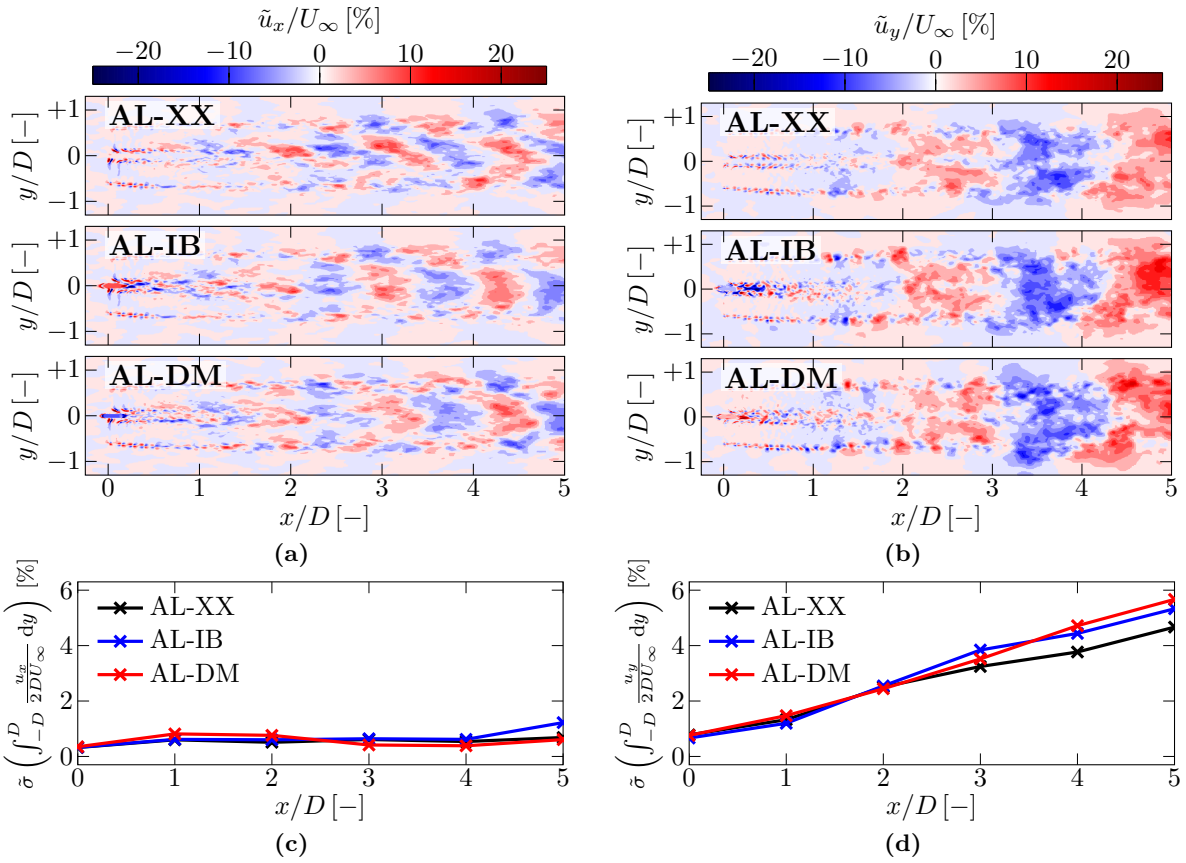

Figure 9. Coherent velocity component contours at $\tau = 0.5$ and coherent standard deviation of the integrated velocity for (a,c) a pitching turbine and (b,d) a rolling turbine with $(f_p^\star, A_p) = (0.60, 1.9°)$ and $(0.30, 1.9°)$, respectively. The planes are located at the initial rotor hub height position.

Figures 9a and 9b depict the coherent velocity for the pitching and rolling turbine cases. As a means to observe the evolution of wake coherence, the velocity component aligned with the direction of platform motion is shown, namely $\tilde{u}_x(\tau)$ for pitching and $\tilde{u}_y(\tau)$ for rolling. In both cases, large-scale coherent structures are observed in the wake as a direct consequence of the platform motions.

Despite the smaller magnitude of platform-induced velocity ($\propto f_p^\star A_p$), the rolling motion generates stronger coherent structures associated with wake meandering, consistent with previous

observations [20]. This is evident from the organised, stripe-like patterns in $\tilde{u}_y(\tau)$. In contrast, pitching motion produces a less organised coherent response, with regions of positive and negative coherent velocity occurring at similar downstream locations, likely due to self-advection of the coherent structures.

For the pitching turbine, differences between the AL-XX, AL-IB, and AL-DM configurations appear to diminish by $5D$, suggesting that the tower and nacelle have a limited influence on wake coherence in this plane, although they may still affect wake evolution and recovery. On the other hand, for the rolling case, the inclusion of the tower and nacelle leads to an amplification of the wake meandering mode. This behaviour is quantified using the coherent standard deviation of the integrated velocity, shown in figures 9c and 9d.

Rolling motions produce modes with consistently higher energy content than those produced by the pitching motions. For pitching, all three modelling approaches yield similar $\tilde{\sigma}$, with only small differences at $1D$ and $5D$. In contrast, for rolling motion, the AL-IB and AL-DM predict a stronger meandering than the AL-XX, indicating that tower and nacelle models may enhance wake meandering. The AL-IB and AL-DM results are in reasonable agreement, although the AL-IB underpredicts the magnitude of the increase, despite its tendency to overestimate tower and nacelle effects. These results demonstrate that the tower and nacelle can have a meaningful influence on wake dynamics, however the magnitude of this influence remains dependent on the platform motion characteristics. It is important to note that the analysis was confined to a single-plane and would be improved upon using a volumetric approach.

3.3. Computational cost

A key consideration in selecting a tower and nacelle modelling approach is the associated computational cost. Using identical numerical schemes and time-step sizes, the average compute time per time step increases by 7.5% and 365% relative to the AL-XX for the AL-IB and AL-DM, respectively. The substantially higher cost of the AL-DM represents a major limitation of body-conforming approaches for floating turbine simulations.

4. Conclusions

This study investigated the influence of tower and nacelle modelling on the aerodynamic response and wake dynamics of a floating wind turbine subject to prescribed platform motions. Two tower and nacelle models, combined with an actuator line representation of the blades, were assessed through comparison with experimental measurements and BR simulations.

All modelling approaches accurately reproduced the coherent rotor thrust response at the platform-motion frequency when compared to both experimental and numerical reference data. However, the actuator line methodology was shown to significantly overpredict tower-shadow effects. While this limits the accuracy of blade-scale loading predictions, comparisons of the wake demonstrated good agreement across methods, indicating that actuator line-based approaches remain suitable for wake-focused studies of floating turbines.

Analysis of wake spectra for a pitching turbine revealed the generation of coherent modes associated with the nacelle, as well as additional spectral content linked to tower shedding. The absence of a nacelle model produced a spurious jet that suppressed coherent dynamics. The IBM and DMM produced broadly similar spectral behaviour, although the characteristic frequency range of the tower-related mode was underpredicted by the IBM. Further downstream, the wake dynamics were dominated by a single coherent mode at the platform frequency.

For the rolling turbine case, time-averaged and coherent wake statistics highlighted the asymmetry generated by the interaction between the tower wake and the rotational motion of the rotor wake. Both the IBM and DMM captured tower-induced coherent fluctuations, with

the IBM predicting a stronger velocity deficit than the DMM. Comparison of coherent velocity structures further demonstrated that, while tower and nacelle modelling had a limited impact on pitching-induced wake modes, they appeared to amplify the wake meandering associated with rolling motions for the selected motion settings. Both modelling approaches showed reasonable agreement in the magnitude of this amplification, indicating a consistent response across the two methods. The distinction between pitching and rolling platform motions highlights the presence of a complex relationship between platform motion settings and the tower and nacelle's influence on the wake.

Finally, a comparison of computational cost showed that the DMM incurs a substantially higher expense than the IBM, highlighting a key practical limitation of body-conforming approaches for floating turbine simulations.

Future work will aim to further quantify the complex interplay between platform motion characteristics and tower and nacelle induced wake dynamics. Extending this analysis to operational-scale turbines, for which the relative size and thus influence of the support structure may be reduced, represents an important direction for future work.

Acknowledgements

The authors gratefully acknowledge Stefano Cioni and Alessandro Bianchini for providing data and further details regarding their CFD study [19].

This work used the ARCHER2 UK National Supercomputing Service through the EPSRC Access to HPC project, Wake Aerodynamics of Offshore Wind Turbines. The authors acknowledge support from DG's EPSRC studentship (no. EP/S023801/1) and CRV's UKRI Future Leaders Fellowship (no. MR/V02504X/1).

References

[1] Edwards E C *et al.* 2023 *Renewable and Sustainable Energy Reviews* **183** 113416
[2] Sørensen J N and Shen W Z 2002 *Journal of Fluids Engineering* **124** 393–399
[3] Cioni S *et al.* 2023 *Wind Energy Science* **8** 1659–1691
[4] Bergua R *et al.* 2023 *Wind Energy Science* **8** 465–485
[5] Pagamonci L *et al.* 2025 *Wind Energy Science* **10** 1707–1736
[6] Santoni C *et al.* 2017 *Wind Energy* **20** 1927–1939
[7] Foti D, Yang X, Shen L and Sotiropoulos F 2019 *Journal of Fluid Mechanics* **869** 1–26
[8] Abraham A *et al.* 2019 *Journal of Wind Engineering and Industrial Aerodynamics* **193** 103981
[9] Zormpa M, Vogel C R and Willden R H J 2026 *Wind Energy* **29** e70077
[10] De Cillis G *et al.* 2021 *Wind Energy* **24** 609–633
[11] Fontanella A *et al.* 2025 *Wind Energy Science* **10** 1369–1387
[12] Poletto R, Craft T and Revell A 2013 *Flow, Turbulence and Combustion* **91** 519–539
[13] Nicoud F and Ducros F 1999 *Flow, Turbulence and Combustion* **62** 183–200
[14] Wimshurst A and Willden R H J 2017 *Wind Energy* **20** 815–833
[15] Willden R *et al.* 2023 *Proceedings of the European wave and tidal energy conference* vol 15
[16] Green D, Zormpa M and Vogel C 2025 *11th Conference on Computational Methods in Marine Engineering*
[17] Schluntz J and Willden R H J 2015 *Wind Energy* **18** 1469–1485
[18] Sotiropoulos F and Yang X 2014 *Progress in Aerospace Sciences* **65** 1–21
[19] Cioni S *et al.* 2025 *Ocean Engineering* **341** 122746
[20] Messmer T, Hölling M and Peinke J 2024 *Journal of Fluid Mechanics* **984** A66